Numerical and experimental study of initiation and propagation of desiccation cracks in clayey soils

Hector U. Levatti[1], Pere C. Prat[2] and Alberto Ledesma[2]

[1]Division of Civil & Building Services Engineering, London South Bank University, London, UK
[2]Dept. of Civil and Environmental Engineering, UPC-BarcelonaTech, Barcelona, Spain

ABSTRACT: This paper presents the fundamentals and the mathematical formulation to study desiccation cracking in soils based on Unsaturated Soil Mechanics as well as a numerical analysis of a previous desiccation test program. The numerical approach implemented in MATLAB is used in 2D simulations on radial sections of the cylindrical specimens and in a theoretical study of the stress field in plane strain conditions. The numerical analysis, based on two stress stare variables (total net stress and suction) is consistent and in good agreement with the experimental results, including the location of cracks and time of crack initiation.

Keywords: desiccation cracking, hydro-mechanical coupling, unsaturated soils mechanics, Finite Element Method.

1. Introduction

Crack desiccation in soils is an important issue because of its implications in a wide range of ground-related fields, from geotechnical engineering to agricultural land use, mining and radioactive waste storage, tailings reservoirs, gravity dams or public buildings [1-5].

The crack patterns that form as the soil dries seems to be random and unique. The cracking process in soils is difficult to reproduce numerically because many features involved are complex and yet not well understood. Formation and propagation of drying cracks in soils involve desiccation (moisture loss) and shrinkage (deformation). This is a coupled hydro-mechanical problem, further complicated because the soil has a highly nonlinear material behaviour in both, the hydraulic and the mechanical components, and most of the soil properties that play a substantial role in the cracking process change with suction or moisture content. In addition to that, boundary conditions (soil-atmosphere interactions or soil-container interactions) are difficult to handle and not yet well understood.

1

Two main variables that play a fundamental role in the formation and propagation of desiccation cracks are the temperature and relative humidity of the environment, but several other factors are involved in the process. In laboratory tests, specimen size, soil-container interface, drying rate and specimen's characteristics (such as heterogeneity, anisotropy, imperfections, water content, particle size, tensile strength or fracture toughness) determine how cracking develops. Additionally, in the field, the soil fabric, the location of the water table, wind velocity, solar radiation, etc. need to be considered as well [6].

When the soil is dried under laboratory conditions or in an environmental chamber, the first cracks that can be seen on the top surface of the specimen are usually boundary cracks that start at the interface between the soil mass and the container wall. These cracks propagate until the entire soil mass is separated from the wall. Soils subjected to cyclic desiccation and wetting experience several phases that start with the soil wet and usually saturated. After the first phase of evaporation, the natural tendency for the specimen is to shrink followed by cracking, resulting in a less wet soil which is usually unsaturated. After the cycle is completed, the soil in the specimen is not saturated, and additional deformation and cracking may develop [7].

The boundary conditions for this problem are complex because they may change during the analysis as the specimen conditions change. The displacement boundary conditions are governed by the friction between container and specimen. Because of the soil's water content changes during the process, the soil/container friction conditions also change and, therefore, the mechanical boundary conditions must be updated during the process. On the other hand, new cracks create new boundaries that are in contact with the environment generating changes in the hydraulic boundary conditions in terms of suction that must also be updated during the evolution of the desiccation process.

Shrinkage occurs when suction increases because of capillary effects. The capillary forces, produced by the suction increment, make the soil mass shrink reducing the size of the pores and consequently the volume of the soil specimen. This may happen in saturated, at the beginning of the process, or unsaturated conditions after a certain time. At the same time, the increasing suction increases the stiffness and the tensile strength [8-10]. If shrinkage is restricted, then cracking develops [6]. Restrictions to shrinkage may be due to three causes: 1) stress or displacement boundary conditions (e.g. friction, adherence with the soil

container); 2) concentration of stresses in the soil matrix; or 3) heterogeneity, texture and soil structure [11].

Desiccation cracks appear both in saturated and unsaturated conditions [12], which is problematic when the state stress variables need to be defined. In fact, the behaviour of the soils at the beginning of the process is more similar to a liquid with no tensile strength. When the soil acquires consistency, tensile strength develops because of the increment in suction. This increment produced by the water loss induces one-dimensional vertical shrinkage at the beginning and a three-dimensional shrinkage when the soil becomes stiffer.

From the experimental point of view, several authors have studied this process since the early twentieth century [13-23] and many significant experimental and numerical contributions have been made in the last half-century [2, 7, 24-38]. An exhaustive state of the art can be found in the doctoral theses of M.R. Lakshmikantha and H. Levatti [7, 12]. However, until the development of Unsaturated Soil Mechanics, the problem has not been analysed considering the parameters that govern the behaviour of soil in the unsaturated state, primarily suction. Tensile strength, which is suction dependent, and fracture toughness are shown to be also relevant parameters [25, 31].

In the context of desiccation cracking, there are numerical approaches available in the literature based on the finite element method (FEM) [2, 28, 39], the finite difference method (FDM) [28], the discrete element method (DEM) [40], the distinct element method (DiEM) [41], the mesh fragmentation technique (MFT) [42], the lattice spring model (DLSM) [43]. However, there is not a consensus on how to properly simulate desiccation cracking in soils due to the number of variables, boundary conditions and complexities involved.

The model presented in this paper is formulated within the classical theories of unsaturated soil mechanics and strength of materials. The flow in deformable porous media is formulated using a coupled hydro-mechanical approach and solved using the finite element method with a $u - p$ formulation [44]. For the crack treatment, a release-node technique is used and simulations show the capabilities of the approach. The proposed model solves the three main physical processes involved (desiccation, shrinkage and cracking). From the initiation of the process, the initial and boundary conditions are fixed and the system evolves until the first crack appears when the tensile strength is reached. The release-node technique

allows dealing with the crack propagation changing the boundary conditions at the crack surfaces.

In the present work and in order to simplify the analysis the thermal component is not considered, assuming that the process is isothermal. Also for the sake of simplicity, a nonlinear elastic constitutive model base on the stress state surface concept [45, 46] is chosen, where the stress variables are suction and net stress. The hydro-mechanical coupling is obtained through the constitutive law and a non-symmetric global system of equations is obtained when solving the problem by the finite element method.

The main objective of the numerical analysis is to reproduce the time evolution of the recorded variables (suction, water content, deformation) during laboratory tests performed in recent years [12, 53] and to estimate the stress evolution before and after the initiation of the cracks. The formulation presented in this work is general [48] but the implementation for the analysis is made in order to solve a radial section of a cylindrical specimen, of 80 cm in diameter and 20 cm in height. The numerical analysis is carried out to simulate the formation and propagation of the first crack, which usually appears at the interface soil-container and initiates from the upper external surface of the specimen and propagates toward the bottom along the interface.

With this technique, only the tensile strength is necessary to be determined in the laboratory. Although linear elastic fracture mechanics (LEFM) has been proposed as an approach to model desiccation cracking in soil by several authors [2, 17, 49, 50], this technique is more complex to implement and the fracture parameters for soils are difficult to obtain because they are dependent on the water content. Apart from that, there is an increasing evidence that the Mohr-Coulomb failure criterion may apply also for this type of problems [25], but this approach will be considered in future developments.

The model presented in this paper is consistent, relatively simple and based on classical theories in the context of geotechnical engineering instead of adding additional numerical items to solve the complexity of the problem. However, complexity can be added gradually.

2. Materials and methods

The soil studied in this work is the Barcelona silty clay that has been used extensively in the past and it has been thoroughly characterized [12, 47, 51]. The method is based on the

observation and measurement of variables during the tests followed for 2D simulations calibrated and validated with the experiment. The specimens used in the experimental program analysed here were moulded into cylindrical PVC containers of and 80 or 40 cm in diameter and 20 or 10 cm in height.

2.1. The experimental program used for the study

The tests were carried out in an existing environmental chamber [12, 52] which was extensively refitted and modified to allow cyclic environmental changes [7, 53]. The main features of this environmental chamber include: a) automatic photography of the external upper surface of the specimen at pre-defined regular intervals; b) halogen lamps to control the chamber temperature; c) data acquisition and control system to record and drive chamber temperature and relative humidity, and suction and temperature of the soil; d) dehumidification system to induce desiccation; e) humidification system to induce wetting; f) control system to combine dehumidification and humidification devices; g) complementary data acquisition system to monitor temperature and volumetric water content of the specimens. Besides recording the images of the cracking patterns that develop on the external surface during the tests, it is possible to detect internal cracks by means of an external ground penetrating radar scanning device [7, 53, 54].

To prepare the tests, the dry soil was first passed through the #16 sieve (1.18 mm opening) and left at laboratory conditions for moisture stabilization. Then the specimens were made at the specified moisture content by adding distilled water. Immediately after mixing the actual moisture content was determined and the mixture was left in a humid chamber for 24 hours before testing.

2.2. Mathematical formulation and numerical approach

In this paper, a hydro-mechanical model is proposed including a released node technique to simulate the desiccation cracking process.

2.2.1. Mechanical constitutive formulation

For the mechanical component of the model, a nonlinear elastic constitutive equation based on the concept of state surfaces [45, 46] is chosen. For the hydraulic component, the

generalized Darcy's law is used and the relation between suction and the degree of saturation is modelled using van Genuchten's closed form expression [55].

In this work, a set of two separated stress variables is introduced, the net stress and the suction [56-60]. The net stress $\boldsymbol{\sigma}^{net}$ (stress in excess of air pressure) and the suction s are:

$$\boldsymbol{\sigma}^{net} = \boldsymbol{\sigma} - u_a \mathbf{1} \tag{1}$$

$$s = u_a - u_w \tag{2}$$

where $\boldsymbol{\sigma}$ is the total stress tensor, u_a and u_w are the air and water pressure respectively and $\mathbf{1} \equiv \delta_{ij}$, is the identity tensor.

2.2.2. Stress-strain-suction relations

For oedometric and triaxial deformation and considering only a desiccation process (no wetting or flooding), which is the case of the tests involved in the analysis, a nonlinear elastic constitutive approach is enough to characterize the changes in volume and the development of stresses in the soil mass. The state surfaces [45, 46] are experimental surfaces (see Figure 1) in the net mean stress – suction – void ratio $\{\sigma_m^{net}, s, e\}$ space, obtained after triaxial tests. Every surface is unique for every soil and it is a soil property. In this case, the state surface is expressed by Eq. (3) is used:

$$\Delta e = a_1 \Delta \ln(\sigma_m^{net} + a_4) + a_2 \Delta \ln\left(\frac{s + p_{ref}}{p_{ref}}\right) + a_3 \Delta\left[\ln(\sigma_m^{net} + a_4)\ln\left(\frac{s + p_{ref}}{p_{ref}}\right)\right] \tag{3}$$

where Δe is the void ratio increment, $\{a_1, a_2, a_3, a_4\}$ are state surface parameters calibrated from laboratory tests, σ_m^{net} is the mean net stress and p_{ref} is a reference pressure to avoid logarithm indeterminacy. In the desiccation problem, deformations occur as a consequence of the decrease of void ratio triggered by increments of suction.

2.2.3. Stress-strain relation

Because of the non-linearity of the material behaviour, the general strain-stress relation must be written in the differential form, Eq. (4):

$$d\boldsymbol{\sigma} = \mathbf{D}d\boldsymbol{\varepsilon} \tag{4}$$

where **D** is the 4th order tangent stiffness tensor. Considering the additive deformation hypothesis, the deformations can be calculated by adding a component due to the net stress and a component due to the suction:

$$d\boldsymbol{\varepsilon} = d\boldsymbol{\varepsilon}^{net} + d\boldsymbol{\varepsilon}^s = \mathbf{C}(\mathbb{K},\mathbb{G})d\boldsymbol{\sigma}^{net} + \mathbf{h}(\mathbb{K}^s)ds \tag{5}$$

where **C** is the 4th order compliance tensor, and **h** is a 2nd order tensor related to changes in suction. $\mathbb{K}$ and $\mathbb{G}$ are the volumetric and shear modulus of the soil matrix, and $\mathbb{K}^s$ is the volumetric suction modulus

The net stress increments can be obtained from (5):

$$d\boldsymbol{\sigma}^{net} = \mathbf{C}^{-1}(d\boldsymbol{\varepsilon} - \mathbf{h}(\mathbb{K}^s)ds) = \mathbf{D}(d\boldsymbol{\varepsilon} - \mathbf{h}(\mathbb{K}^s)ds) \tag{6}$$

where $\mathbf{D} = \mathbf{C}^{-1}$, is the tangent stiffness tensor.

The compliance and stiffness tensors depend on the volumetric and shear modulus $\mathbb{K}$ and $\mathbb{G}$, while the suction tensor **h** depends on the volumetric suction modulus $\mathbb{K}^s$. These material properties ($\mathbb{K}, \mathbb{G}, \mathbb{K}^s$) are not constant, since the volumetric strain depends on the state surface. Then from Eq. (3):

$$\varepsilon_v = -\frac{\Delta e}{1+e_0} = -\frac{1}{1+e_0}\left\{ a_1\Delta\ln(\sigma_m^{net}+a_4) + a_2\Delta\ln\left(\frac{s+p_{ref}}{p_{ref}}\right) \right. \\ \left. + a_3\Delta\left[\ln(\sigma_m^{net}+a_4)\ln\left(\frac{s+p_{ref}}{p_{ref}}\right)\right] \right\} \tag{7}$$

In the same way that the total strain increment can be decomposed into net strain and suction strain increments, as in equation (5), the volumetric strain can also be decomposed into a net volumetric strain, ε_v^{net}, and a suction volumetric strain, ε_v^s. Incrementally,

$$d\varepsilon_v = d\varepsilon_v^{net} + d\varepsilon_v^s; \quad d\varepsilon_v^{net} = \mathbb{K}_t(\sigma_m^{net},s)d\sigma_m^{net}; \quad d\varepsilon_v^s = \frac{ds}{\mathbb{K}_t^s(\sigma_m^{net},s)} \tag{8}$$

where $\mathbb{K}_t(\sigma_m^{net},s)$ and $\mathbb{K}_t^s(\sigma_m^{net},s)$ are the tangent volumetric and suction nonlinear elastic moduli, respectively, which depend on the mean net stress and on suction. Therefore:

$$d\varepsilon_v = \mathbb{K}_t(\sigma_m^{net},s)d\sigma_m^{net} + \frac{ds}{\mathbb{K}_t^s(\sigma_m^{net},s)} \tag{9}$$

On the other hand, $d\varepsilon_v$ can also be calculated as

$$d\varepsilon_v(\sigma_m^{net}, s) = \frac{\partial \varepsilon_v}{\partial \sigma_m^{net}} d\sigma_m^{net} + \frac{\partial \varepsilon_v}{\partial s} ds \qquad (10)$$

Comparison of Eq. (9) and Eq. (10) shows that the volumetric moduli are the partial derivatives of the state surface with respect to the mean net stress and suction respectively:

$$\frac{\partial \varepsilon_v}{\partial \sigma_m^{net}} = \mathbb{K}_t(\sigma_m^{net}, s)$$

$$\frac{\partial \varepsilon_v}{\partial s} = \frac{1}{\mathbb{K}_t^s(\sigma_m^{net}, s)} \qquad (11)$$

The tangent elastic moduli can then be obtained from Eq. (11) in terms of the state surface parameters a_1, a_2, a_3, a_4, and the stress variables σ_m^{net} and s:

$$\mathbb{K}_t(\sigma_m^{net}, s) = \frac{-a_1 - a_3 \ln\left(\frac{s + p_{ref}}{p_{ref}}\right)}{(1 + e_0)(\sigma_m^{net} + a_4)}$$

$$\mathbb{K}_t^s(\sigma_m^{net}, s) = \frac{(1 + e_0)(s + p_{ref})}{-a_2 - a_3 \ln(\sigma_m^{net} + a_4)} \qquad (12)$$

Assuming that the air pressure is constant and equal to zero, $u_a = 0$, the elastic moduli can be written in terms of the effective mean stress p' and the negative porewater pressure $-u_w$:

$$\mathbb{K}_t(p', u_w) = \frac{-a_1 - a_3 \ln\left(\frac{-u_w + p_{ref}}{p_{ref}}\right)}{(1 + e_0)(p' + a_4)}$$

$$\mathbb{K}_t^s(p', u_w) = \frac{(1 + e_0)(-u_w + p_{ref})}{-a_2 - a_3 \ln(p' + a_4)} \qquad (13)$$

For simplicity and because the deformation produced by the increment of suction is mainly volumetric, a constant Poisson's ratio and the linear elastic relation between the shear and Young's moduli are adopted:

$$\mathbb{G}_t = \frac{3K_t(1 - 2v)}{2(1 + v)} = \frac{3(1 - 2v)(1 + e_0)(p' + a_4)}{2(1 + v)\left[-a_1 - a_3 \ln\left(\frac{-u_w + p_{ref}}{p_{ref}}\right)\right]} \qquad (14)$$

The volumetric deformation produced by changes of suction is then

$$d\varepsilon_v^s = -\frac{1}{\mathbb{K}_t^s(p', u_w)} du_w \tag{15}$$

and the stress-strain relation becomes

$$d\sigma_{ij} = C_{ijkl}\left(d\varepsilon_{kl} - \frac{d\varepsilon_v^s}{3}\delta_{kl}\right) = C_{ijkl}\left(d\varepsilon_{kl} + \frac{du_w}{3K_t^s}\delta_{kl}\right) \tag{16}$$

Finally, in matrix form, the stress-strain relation is

$$d\boldsymbol{\sigma} = \mathbf{D}(d\boldsymbol{\varepsilon} - d\boldsymbol{\varepsilon}^s) = \mathbf{D}\left(d\boldsymbol{\varepsilon} + \mathbf{m}\frac{du_w}{3K_t^s}\right) \tag{17}$$

where $\boldsymbol{\varepsilon}^s$ is the spherical tensor of deformations due to suction ($\varepsilon_{ij}^s = u_w\delta_{ij}/K_t^s$) and $\mathbf{m} = [1 \quad 1 \quad 1 \quad 0 \quad 0 \quad 0]^T$ is the identity tensor in vector form. The stiffness matrix $\mathbf{D}$ corresponds to an isotropic non-linear elastic material (volumetric and shear deformations are uncoupled).

2.2.4. Hydraulic constitutive formulation

The generalized Darcy's law for unsaturated soils is expressed as:

$$\mathbf{q} = -\mathbf{K}(S_r) \cdot (\nabla u_w - \mathbf{g}\rho^w) \tag{18}$$

where $\mathbf{q}$ is Darcy's velocity vector; ∇u_w is the porewater pressure gradient; $\mathbf{K}(S_r)$ is the permeability tensor which depends on the water saturation degree (S_r); $\mathbf{g}$ is the gravity vector and ρ^w is the water density.

The permeability tensor is written in terms of the intrinsic permeability as:

$$\mathbf{K}(S_r) = \mathbf{k}(n)\frac{k^{rl}(S_r)}{\mu^l} \tag{19}$$

where k^{rl} is the non-dimensional relative permeability, with values in the range 0 to 1, that depends on the degree of saturation (here $k^{rl} = (S_r)^r$, with constant r, is adopted); μ^l is the temperature-dependent dynamic viscosity of water; $\mathbf{k}(n) = (\mu^l/\gamma_w)K\mathbf{1}$ is the intrinsic permeability tensor (a material property), which is a function of the porosity and of the viscosity and temperature of the fluid; γ_w is the specific weight of water; and K is the hydraulic conductivity of the soil. For isotropic permeability, the permeability is a scalar. In the case of orthotropic or axial symmetry the permeability tensor could be diagonal.

In case of hydro-mechanical coupling, it is necessary to relate the saturated hydraulic conductivity to changes of porosity. For that purpose, the following exponential law can be used:

$$k_{sat} = k_0 \exp[b(n - n_0)] \tag{20}$$

where k_0 is the saturated hydraulic conductivity of reference at $n = n_0$, k_{sat} is the saturated hydraulic conductivity for porosity n, and b is a material parameter. For saturated soils, $K = k_{sat}$.

The water retention curve of the soil is known from previous research [47] and was obtained using the psychrometric technique. The van Genuchten function [55] was used in the analysis:

$$S_r = \left[1 + \left(\frac{s}{P_0 \cdot f_n} \right)^{\frac{1}{1-\lambda}} \right]^{-\lambda} \tag{21}$$

$$f_n = \exp[-\eta(n - n_0)] \tag{22}$$

where λ is a material parameter; P_0 is the air entry value for the initial porosity n_0, adopted as a reference value; f_n is a function that takes into account the influence of porosity in the retention curve by means of parameter η. The parameters corresponding to this function and to the soil used are given in Table 2.

2.3. Finite element approximation

The formulation corresponds to a one-phase flow in a deforming unsaturated porous media problem (Richard's problem, [61]). The finite element method is used for the discretization in space and the finite difference method for the time discretization. The unknown variables in this problem are the porewater pressure, $u_w(\mathbf{x}, t)$, and the displacements $\mathbf{u}(\mathbf{x}, t)$.

Because of the hydro-mechanical coupling of this problem, a *u-p* formulation [44] is adopted, where $\mathbf{u}$ are the nodal displacements and $\mathbf{p}$ is the nodal negative porewater pressure. After the application of the finite element method, the coupled desiccation problem is expressed as a system of partial differential equations:

$$\begin{cases} \mathbf{K}_{\mathrm{T}}\dfrac{\partial \bar{\mathbf{u}}}{\partial t} + \mathbf{Q}_{\mathrm{T}}\dfrac{\partial \bar{\mathbf{p}}}{\partial t} = \dfrac{\partial \mathbf{f}^{u}}{\partial t} \\[3mm] \mathbf{P}\dfrac{\partial \bar{\mathbf{u}}}{\partial t} + \mathbf{S}\dfrac{\partial \bar{\mathbf{p}}}{\partial t} + \mathbf{H}\bar{\mathbf{p}} = \mathbf{f}^{p} \end{cases} \tag{23}$$

Where $\mathbf{K}_{\mathrm{T}}$ is the global stiffness matrix, $\mathbf{Q}_{\mathrm{T}}$ and $\mathbf{P}$ are coupling matrices, $\mathbf{S}$ is a compressibility matrix and $\mathbf{H}$ is the permeability matrix.

In matrix notation, the system of partial differential equations (23) can be written as:

$$\begin{bmatrix} \mathbf{0} & \mathbf{0} \\ \mathbf{0} & \mathbf{H} \end{bmatrix}\begin{bmatrix} \bar{\mathbf{u}} \\ \bar{\mathbf{p}} \end{bmatrix} + \begin{bmatrix} \mathbf{K}_{\mathrm{T}} & \mathbf{Q}_{\mathrm{T}} \\ \mathbf{P} & \mathbf{S} \end{bmatrix}\begin{bmatrix} \dfrac{d\bar{\mathbf{u}}}{dt} \\ \dfrac{d\bar{\mathbf{p}}}{dt} \end{bmatrix} = \begin{bmatrix} \dfrac{d\mathbf{f}^{u}}{dt} \\ \mathbf{f}^{p} \end{bmatrix} \tag{24}$$

which is the typical form of hydro-mechanical problems in unsaturated soils [70].

The derivation using separated variables produces a non-symmetric system of equations because $\mathbf{Q}_{\mathrm{T}} \neq \mathbf{P}$. The coupling of the mechanical and hydraulic problem is materialized by the mechanical constitutive equation (17), which links the pore water pressure (hydraulic variable, u_w) with the total stress (mechanical variable, $\boldsymbol{\sigma}$). The *u-p* formulation [44] is summarized in the Appendix.

2.4. Release node technique

Desiccation of soils is usually followed by cracking [2, 12, 18]. There are three main quantities that need to be discussed to simulate the crack formation and propagation: the stress level at crack initiation (σ_c), the direction of crack propagation (θ_c), and the crack propagation length (Δa). These three issues need to be solved in the context of the finite element analysis by implementing an appropriate solution algorithm. In a continuum mechanics framework, crack propagation implies a change of the boundary value problem, because new boundaries (crack faces) are generated with modified conditions. In the proposed technique, crack propagation is modelled as a temporal sequence of boundary value problems with discrete growing crack lengths, a_i, and a material separation along the crack increment Δa_i is assumed to be discontinuous. In reality, crack propagation occurs continuously and the failure of the material in the process zone is a continuous process too. Clearly, there is a difference between the material model and the numerical technique, but this is a necessary approximation for the numerical analysis [62].

The stress level when cracking starts corresponds to the tensile strength of the soil in a traditional strength of material approach [63]. The process of desiccation in the laboratory starts with the soil as a slurry with no tensile strength. Once the soil acquires consistency, because of suction increments, the tensile strength increases until reaching a maximum and after that, it decreases with further increments of suction [12].

The direction of crack propagation is perpendicular to the maximum principal tensile stress and, for simplicity, the amount of propagation is assumed to be equal to the length of the finite element.

In Figure 2 (stages a, b, c and d), the procedure to initiate and propagate a crack in the boundary is shown. Stages e, f, g and h show the procedure to be applied for a generic crack that starts in the surface of the soil. Assuming that during the course of a finite element analysis the failure criterion is reached at a point, and the amount of crack propagation, Δa, is equal to the length of the element, the node release algorithm is as follows:

1. Keep the external loads constant (suction profile, Figure 2a)
2. Determine the reactions, R_i, or inter-elements forces, F_i (Figure 2a)
3. Release the nodal bonding and split the nodes (Figure 2b or f)
4. Replace the bond at the released node by an equivalent force R (reaction) or F (inter-element force), (Figure 2b or f)
5. Release stepwise the force from R to zero and add proportionally suction to the new node exposed to the environment (Figure 2c or g).
6. Check whether the failure criterion is fulfilled at the new crack length:
   - if yes, unstable crack propagation, go to 2
   - if no, continue the finite element analysis with the next load step (Figure 2d or h)

This technique is especially useful when the crack propagation path is known, as is the case in some of the cracks in laboratory tests. For more arbitrary cracks this technique is mesh-dependent. This method permits to know the stress state in the soil matrix during the desiccation process which is the key to define the initiation of the cracks and their propagation.

In the soil under desiccation, the direction of the crack depends on several intrinsic factors: heterogeneity, anisotropy, imperfections, impurities, plasticity, the initial water content, the initial particle size, the tensile strength, the fracture toughness and the fabric in the

field. In the future, it will be necessary to include all these factors in the model in order to study their influence on the numerical results and compared to experimental data.

3. Results and discussion

The tests presented are from a previous desiccation experimental programs [12] and from a cyclic experiment of the authors of this paper [53], to investigate the behaviour of the specimens in an environmental chamber. The cyclic test includes five stages: first drying, first wetting, flooding, second drying and second wetting. A summary of all those results is included to have a broader understanding of the phenomenon under analysis.

3.1. Results of the test program

Table 1 contains a summary of the results from the tests described above [12] and [53].

The results show that the first cracks in this kind of cylindrical specimens (80/40 cm in diameter and 20/10 cm thick) and conditions (21-45ºC and 30-85% RH) start at the soil/container interface sometime during the first week of the test. The initiation of a crack is certainly difficult to detect and predict because it can originate practically anywhere [7, 53, 54]. Crack patterns show cracks triggered by displacement boundary conditions, stress concentrations or material heterogeneity [11]. Suction at the end of the test range from 75 to 150 MPa. Equilibrium was reached at 30 to 120 days of initiation, depending on the specimen size and the environmental conditions (temperature and relative humidity). A significant suction increment was noticed between 10 and 40 days of initiation also depending on specimen size and environmental conditions. These values will be used as boundary conditions in the numerical simulations.

Figure 3 shows the evolution of the suction in specimens of 80 and 40 cm in diameter and 20 and 10 cm of height obtained from previous tests [12]. The 10 cm thick specimens that were tested in the environmental chamber had a very similar suction evolution, with maximum values of suction about 105-110 MPa. These three tests show that temperatures of 35ºC combined with RH of 40% produce, from the beginning, considerable suction increments. However, for temperatures of 21ºC or less the specimens needed several days before showing noticeable suction.

The evolution of the soil moisture the tests is presented in Figure 4. It is clear that the behaviour of the 80×10 specimens in the cyclic test is very similar to the previous tests [12] in terms of moisture loss during the first stage of drying. This fact permits the direct comparison of the other variables (e.g. suction). In all the tests two stages are well observed, a first slow desiccation during the first days with small increments in suction and large values of moisture loss and a faster period with larger increments of suction and small values of moisture loss.

Figure 5 shows the evolution of soil humidity obtained from previous laboratory tests [12]. These results are directly comparable with the results presented as a part of this research because they shared the same type of soil and container, as well as the environmental chamber and conditions. The analysis of the specimens shows several cracks forming at the bottom and propagating partially to the top surface, probably because the presence of sensors generated some restrictions producing a more complex crack pattern. With the use of a ground penetrating radar system [54], the analysis of this specimen showed that there were cracks that started in the middle or bottom of the specimen before becoming visible at the top surface [7, 53].

3.2. Basic assumptions for the numerical analysis

The soil used for the specimens is a low plasticity clay with Atterberg limits $w_S = 2.2\%$, $w_L = 32\%$, $w_P = 16\%$ and plasticity index $PI = 16\%$.

The permeability depends on the dry density, void ratio and degree of saturation. The permeability of the soil used, for dry density between 16.1 kN/m^3 and 17 kN/m^3, and the void ratio between 0.5 and 0.76, has values between 4×10^{-13} m/s and 8×10^{-12} m/s for a degree of saturation between 70% and 40%. The average saturated permeability for a void ratio of 0.48 was of 1×10^{-9} m/s. Figure 6 shows the permeability values obtained in previous works [47] in terms of the degree of saturation S_r.

The tensile strength of soils is an important indicator of material strength, as it depends on other properties of the soil. Until recently, determination of the soil's tensile strength had not received the attention it deserved, mainly because of the difficulty in the experimental setup. The tensile strength of unsaturated soils varies with the degree of saturation (moisture content) and suction as well as with density. In this paper, the prediction of crack initiation and propagation is based on Griffith's approach [64], which is a strength of material

approach. In order to simplify, the prediction of the crack initiation and propagation can be made considering a tensile strength calculated according to [12].

The numerical study presented in this paper is focused only on cracks formed by restricted displacement boundary conditions or by stress concentrations. Specifically, in the first cracks formed in the soil/container interface. Accounting for the influence of heterogeneity needs a material characterization that is beyond the scope of this paper.

The numerical analysis simulates the desiccation process and subsequent cracking from the laboratory tests with a hydro-mechanical formulation discussed in section 3, which has been implemented in a MATLAB code in particular to reproduce the time evolution of the recorded variables (mainly suction and water content) and to estimate the stress evolution before and after the initiation of the cracks. When cracks initiate, a release node technique is activated in order to simulate the crack propagation. The numerical analysis has been made on a radial section of a cylindrical specimen as shown in Figure 7.

In the laboratory test program described in the preceding section, one-dimensional (vertical) shrinkage was observed in all tests during the first stage of the drying process. In the beginning, the soil had a slurry consistency and its mechanical behaviour was close to that of a compressible fluid with negligible tensile or shear strength. After a time, the consistency of the soil changed to solid, resulting in a three-dimensional behaviour where the adherence between the specimen and the container increased. These adherence changes the boundary condition to fixed supports in the soil/container interface, yielding tensile stresses that eventually result in the formation of a perimeter crack and the separation of the soil from the container's wall (Figure 8). After the perimeter crack has fully developed, other cracks appear in the central portion of the specimen.

The values of the parameters for the stress state surface, the retention curve, and the tensile strength, needed for the numerical analysis, were calibrated using the available experimental data for the Barcelona silty clay in the literature [12, 47] and the test program described in the preceding sections. They are summarized in Table 3.

A number of different suction and displacement boundary conditions may be considered in the numerical analyses [7] (Figure 7).

3.3. Crack initiation and propagation of perimeter cracks

The experimental results on cylindrical specimens (80/40 cm diameter and 20/10 cm height) have shown that the first crack forms at the contact between specimen and container, and propagates following the vertical interface. In many cases, the second crack forms near the centre of the specimen and propagate toward the perimeter.

In the radial section used for the numerical analysis, the first crack propagates in a vertical direction from the top to the bottom. Because in this case, the cracks propagate along the vertical border of the radial section, the release-node technique is made simpler: it consists on a displacement and suction boundary condition changing technique (Figure 7). Whenever the tensile strength is reached in a node, the corresponding displacement restriction is released.

Figure 7a shows the radial section used for the analysis (radial section 40 x 20 cm) that correspond to the experiment with a sample of 80 and 20 cm in diameter and height (Figure 3). In this simulation, plane strain state is assumed and self-weight is ignored.

In this analysis, the boundary condition in terms of displacement changes as is shown in Figure 7b, c, d, e and f, when the crack is propagated.

The boundary condition in terms of the porewater pressure is variable in order to reproduce the experimental test (Figure 3), starting with a suction of 5 MPa. After 35 days, the suction is increased to 20 MPa and after 60 days it is finally fixed at 120 MPa. This porewater pressure is applied as well progressively on the contours that are exposed to the environment when a node is released (see red line in Figure 7b, c, d, e and f).

The evolution of the porewater pressure at the reference point (Figure 8d) of the radial section is shown in Figure 8a. The reference point is located at a half height and to a distance of 10 cm from the right border. Changes in the porewater pressure are qualitatively consistent with the laboratory results with cylindrical specimens (Figure 3).

The evolution of the horizontal and vertical stresses, as well as the horizontal and vertical components of the stress-strain relation at three points of the radial section (Figure 8e,f), are shown in Figure 8b,c. The suction field and the horizontal and vertical stress fields in the section after 100 days of desiccation are shown in Figure 8d,e,f. Tensile stresses that can trigger crack initiation develop during the desiccation process at the upper-right corner of the section Figure 8b. The values of the tensile stresses are larger than the assumed tensile strength of 3.5 kPa, leading to crack initiation during the third day of desiccation. The

important fact of this simulation is that the horizontal stress is the maximum stress and it is tension over the tensile strength. On the other hand, the maximum tensile horizontal stress is produced in the right-top corner in correspondence to what was checked in the experiments.

The suction gradients, which are the only source of stresses and deformations, are horizontal and vertical because of the asymmetry of the assumed displacement boundary conditions (Figure 8d). This is a key point for the production of horizontal tensile stresses that initiate the crack in this case [7].

The numerical simulation is consistent with this experimental result in terms of deformation and time evolution. The deformed radial section of the actual sample is shown in Figure 8d after 100 days of desiccation.

Because of the imposed boundary condition, the first stage of one-dimensional shrinkage is captured very well. In this simulation, the analysis includes the use of the release-node technique in order to simulate the initiation and propagation of the first crack at the soil/container interface.

The evolution of the porewater pressure at the reference point is similar to the evolution of the suction recorded during the test for this particular specimen (Figure 3). Figure 4 shows the evolution of the numerically calculated moisture compared with the test results. The results are qualitatively consistent with the experimental measurements, with the first crack propagating from top to bottom of the radial section.

4. Conclusions

This paper describes the theoretical and numerical formulation for the analysis of desiccation cracking in soils. The general model presented includes the influence on the problem of all main variables and features that control the physical process. It is based on fundamental principles of the Unsaturated Soils Mechanics and Strength of Materials and features a good balance between complexity and relatively simple tools for the analysis of desiccation cracking in soils. The main parameters that control the physical process were identified from experimental tests and included in the mathematical formulation to simulate cracking. The resulting relatively simple tool can be used for a better understanding of the process of desiccation cracking in soils. The model is presented for two-dimensional analysis although the formulation is general and the implementation can be easily extended to three dimensions.

Cracking simulation is carried out by means of a "release node" technique, taking into account that cracks generate a new boundary where atmosphere relative humidity and suction must be imposed.

This model can be easily extended to develop other more complex models to explore boundary effects such as the soil-atmosphere and soil-container interaction, as well as simulation of cracking using Fracture Mechanics. The formulation presented in this paper is validated with experimental tests.

The numerical analysis presented in the paper reproduces with a good agreement the behaviour of the soil during the tests. In all the tests a first stage shows one-dimensional shrinkage without cracks, continuing with a second stage consisting of three-dimensional shrinkage resulting in a separation of the soil from the container wall. The model is able to reproduce the main features of the laboratory tests including the three stages: desiccation, shrinkage, and cracking. The separation crack is three-dimensional but from the perspective of the radial section of the specimen used in the numerical analysis, the crack propagates from the top to the bottom of the soil mass.

In an intermediate stage of the process of desiccation, the model predicts a stress field with tensile stresses capable of triggering cracks because the tensile strength is reached in the horizontal direction. The distribution of the horizontal and vertical stress fields may explain why the first cracks to appear are those at the soil/container interface, starting at the top surface of the specimen.

Simulations of initiation and propagation of the first crack show a similar behaviour to laboratory observations, which suggests that the main mechanisms of the physical problem have been considered, including not only the governing equations but also the appropriate boundary conditions.

Acknowledgements

TABLES

Table 1 – Summary of test results with cylindrical specimens from [12] and [53]

Sample Size[1] (cm)	Duration of test (days)	T[4] (ºC)	RH[5] (%)	Contact[6]	Equilib. Time[7] (days)	First crack appears (days)	Saturated period[8] (days)	Humidity at saturation (%)	Significant Suction increment (from day)	Max. suction reached (MPa)
80×10 [2]	32	35	40	NF	30	—	8	—	5	105
80×10 [2]	38	35	40	F	35	8	5	20	5	110
40×10 [2]	46	35	40	F	40	—	15	—	5	150
40×10 [2]	106	21	40	F	40	—	20	12	20	75
80×20 [2]	120	21	40	F	120	8	34	10	40	100
80×10 [3]	55	22-28	30-85	NF	—	8	5	10-20	10	0.1

[1] Diameter × Height [2] Experimental program included in [12]; [3] Experimental program included in [53]; [4] Temperature imposed in the environmental chamber to produce desiccation; [5] Relative Humidity imposed in Chamber to produce desiccation; [6] Contact surface between soil and tray: NF: no friction; F: friction; [7] Time when moisture change in the sample is negligible; [8] Period of time when the sample remain saturated.

Table 2 – Parameters of the water retention curve for Barcelona silty clay [47]

Void ratio (e)	Porosity (n)	γ_d (g/cm³)[1]	$f_n = \exp[-\eta(n-n_0)]$[2]	λ [3]	$1/(1-\lambda)$
0.87	0.47	1.45	1.04	0.27	1.37
0.75	0.43	1.55	1.07	0.25	1.33
0.64	0.39	1.65	1.12	0.23	1.30
0.55	0.35	1.75	1.16	0.20	1.25

[1] γ_d (g/cm³) is the dried unit weight of the soil; [2] f_n is a function that takes into account the influence of porosity in the retention curve by means of parameter η; [3] λ is a material parameter and n_0 is the initial porosity of the soil sample.

Table 3 – Parameters used in the numerical analysis

Mechanical parameters						
a_1 (−)	a_2 (−)	a_3 (−)	a_4 (MPa)	P_{ref} (MPa)	Poisson Ratio ν	σ_c (MPa)
-0.02	-0.0025	-0.000039	0.023	0.1	0.4	0.0035

a_1, a_2, a_3 and a_4 are the state surface parameters Eq. (7); P_{ref} is a reference pressure to avoid logarithm inderterminancy; ν is the possion ratio and σ_c is the tensile strength of the soil.

Hydraulic parameters			
Initial permeability k_0 (m/s)	Material parameter b	Initial porosity n_0	Material parameter r
9.27×10⁻¹⁰	25	0.6	3

The permeability tensor is written in terms of the intrinsic permeability as $\mathbf{K}(S_r) = \mathbf{k}(n)\frac{k^{rl}(S_r)}{\mu^l}$, where k^{rl} is the non-dimensional relative permeability, with values in the range 0 to 1, that depends on the degree of saturation (here $k^{rl} = (S_r)^r$, with constant r, is adopted); μ^l is the temperature-dependent dynamic viscosity of water; $\mathbf{k}(n) = (\mu^l/\gamma_w)K\mathbf{1}$ is the intrinsic permeability tensor (a material property), which is a function of the porosity and of the viscosity and temperature of the fluid.
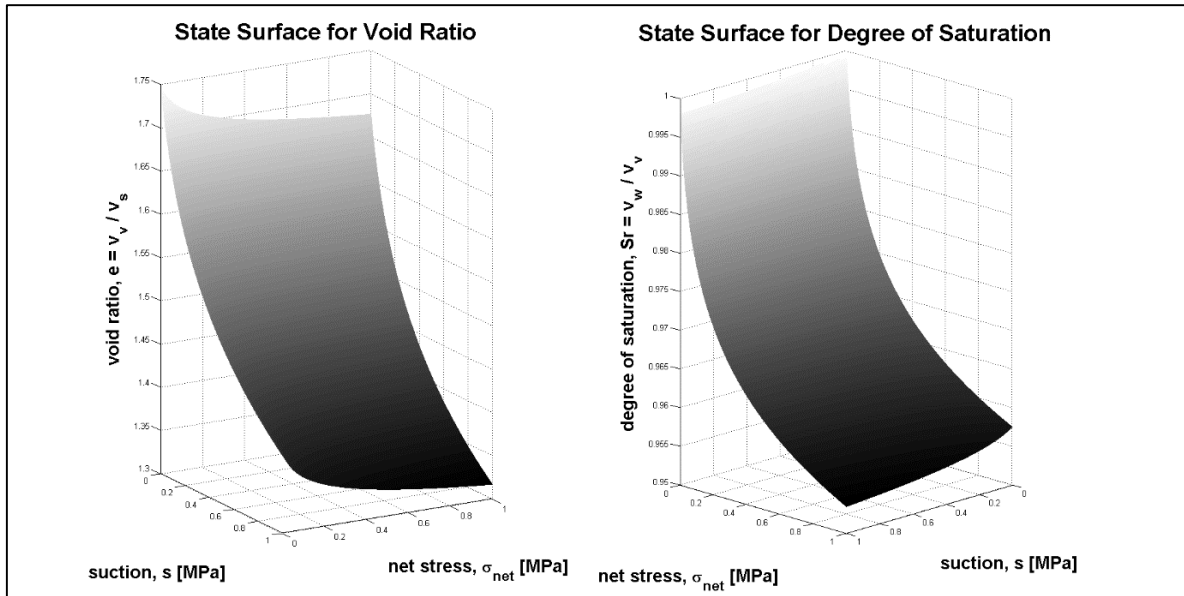
FIGURES

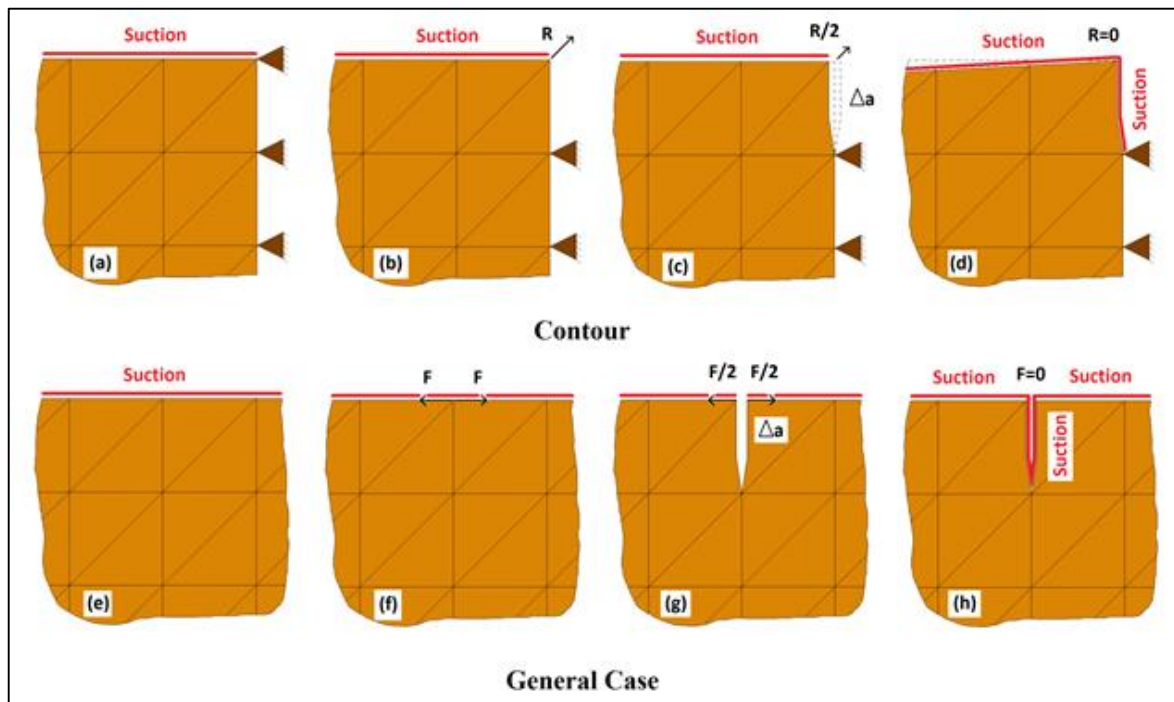Figure 1 – State surfaces from Matyas & Radhakrishna [45] and Lloret & Alonso [46]

Figure 2 – Release node technique. Boundary crack case: a) starting scheme, b) equivalent starting scheme, c) reduction of reaction and progressive application o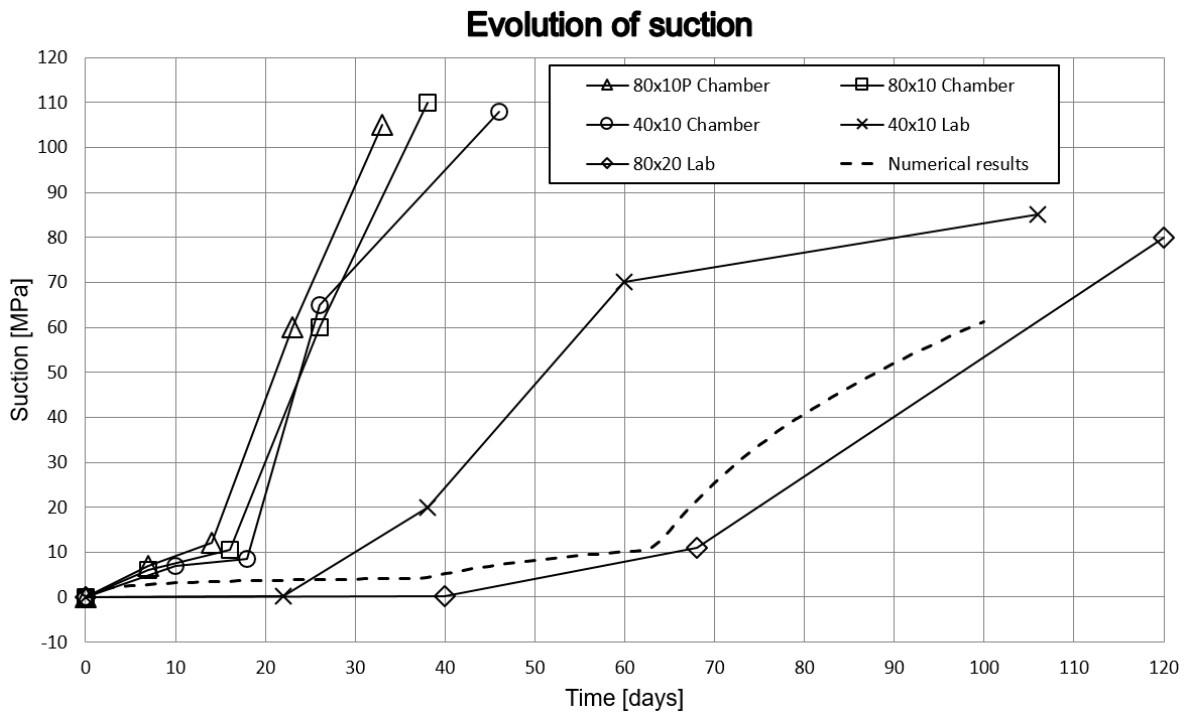f suction, d) final scheme with crack propagated. General crack case: e) starting scheme, f) equivalent starting scheme, g) reduction of forces and progressive application of suction, h) final scheme with crack propagated

Evolution of suction

Figure 3 – Evolution of suction in specimens of 80/40 cm in diameter and 20/10 cm height in laboratory and environmental chamber conditions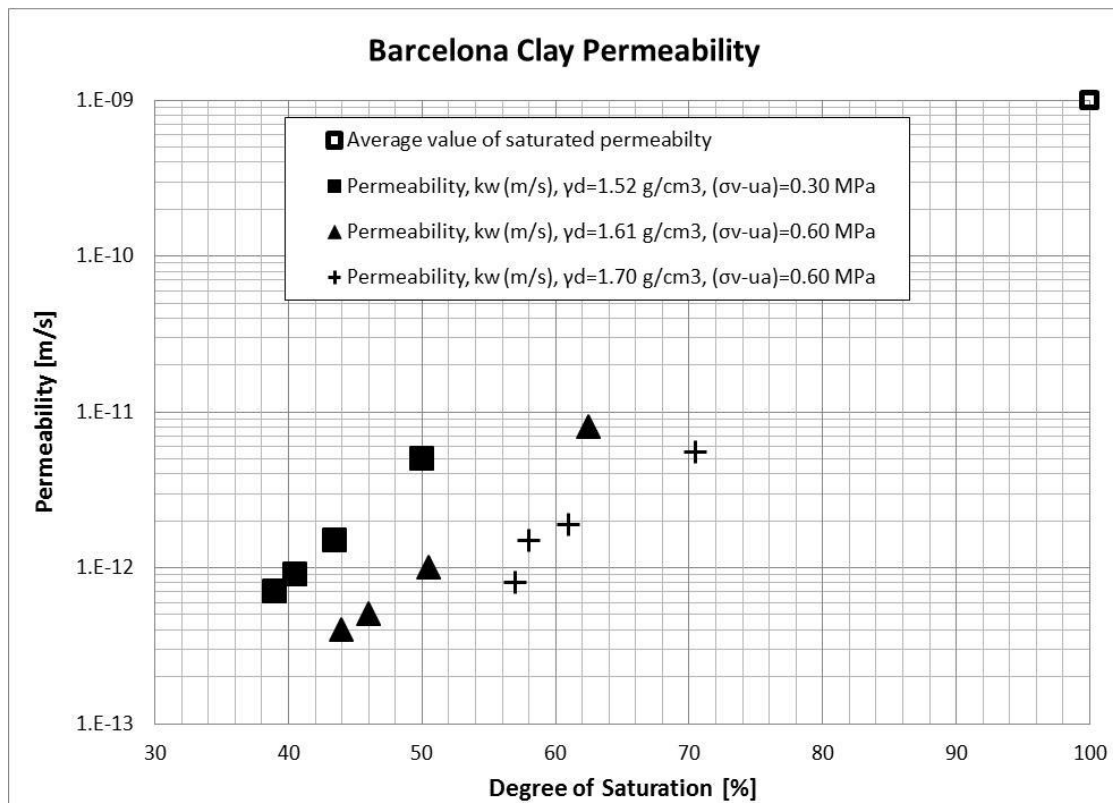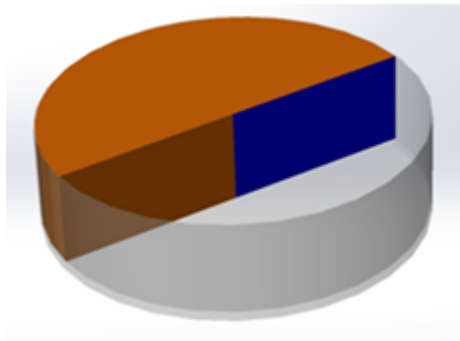 measured in the middle of the sample [12] and comparison with the numerical simulation of radial cross-section 40 cm wide and 20 cm high

Evolution of moisture

Figure 4 – Evolution of moisture (global gravimetric water content) in specimens 80/40 cm in diameter and 20/10 cm height in laboratory and environmental chamber conditions [12, 53] and comparison with the numerical simulation of radial cross-section 40 cm wide and 20 cm high

Figure 5 – Evolution of soil humidity in specimens 80/40 cm in diameter and 20/10 cm height in laboratory and environmental chamber conditions measured in the middle of the sample [12].
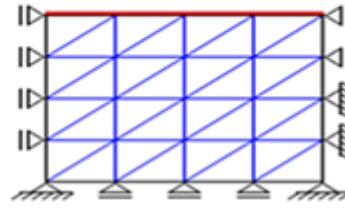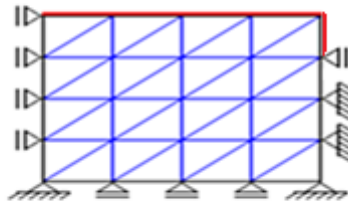

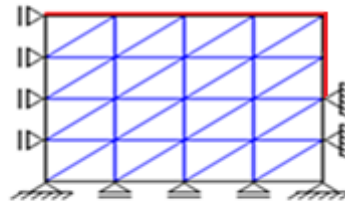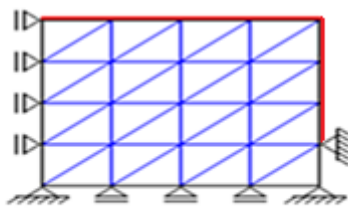
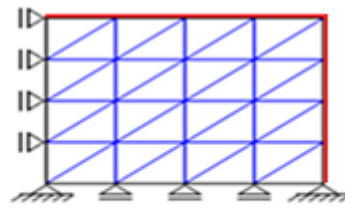Figure 6 – Permeability [47]

(a) Radial section analysed numerically

(b) Initial Stage
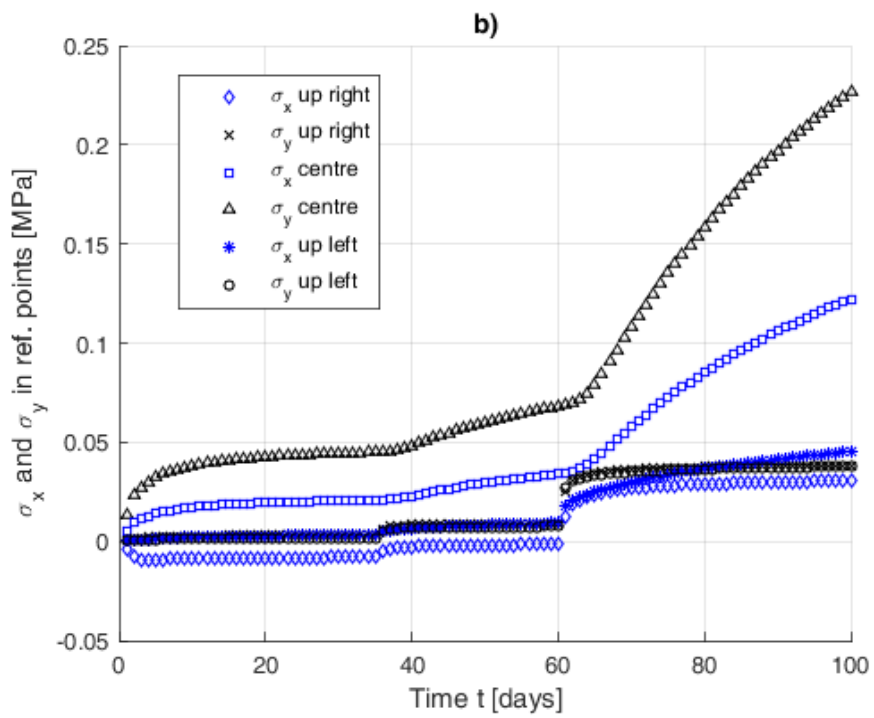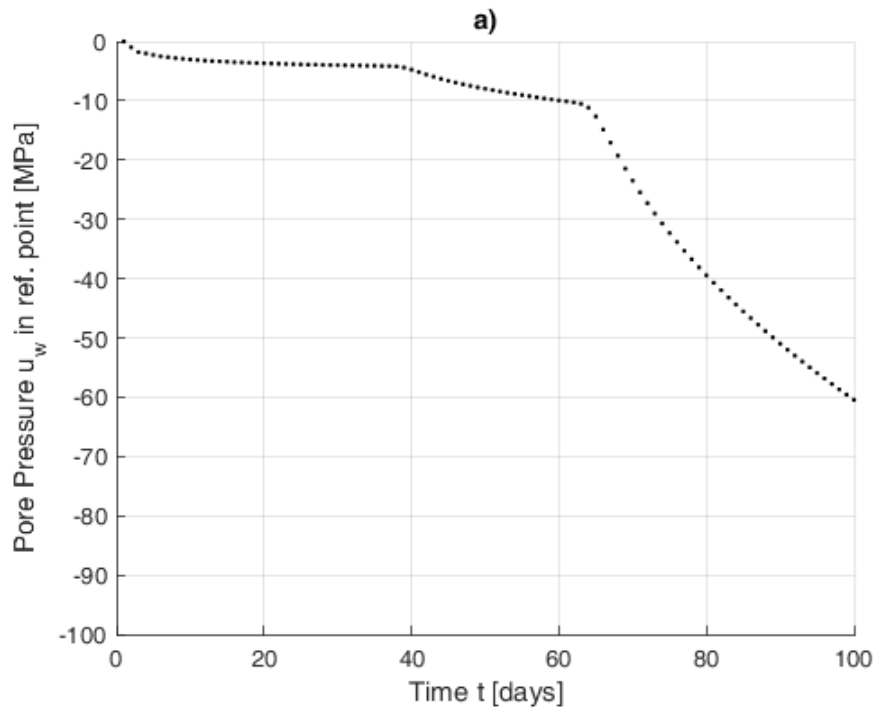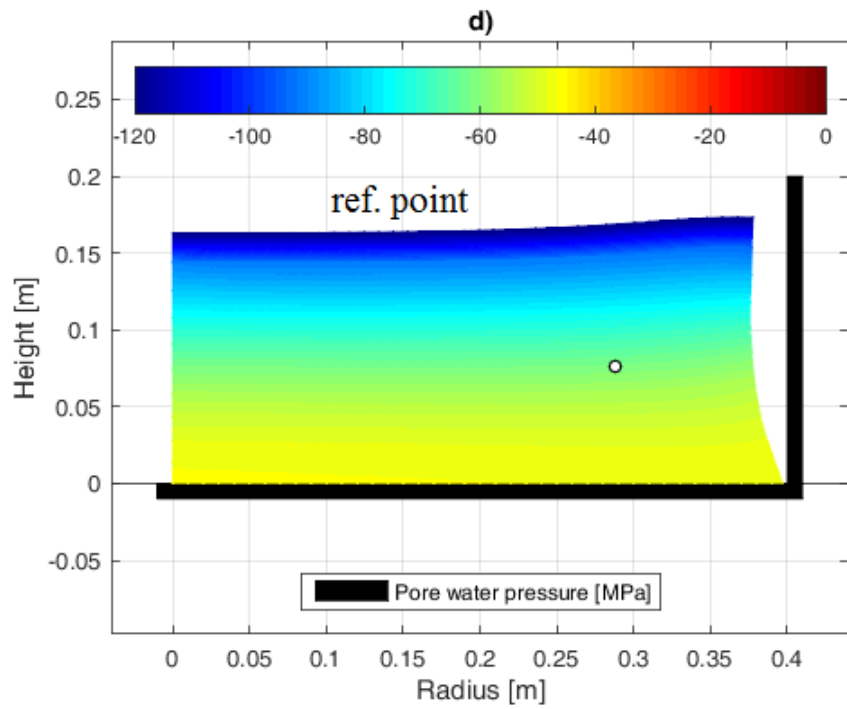
(c) Intermediate Stage

(d) Intermediate Stage

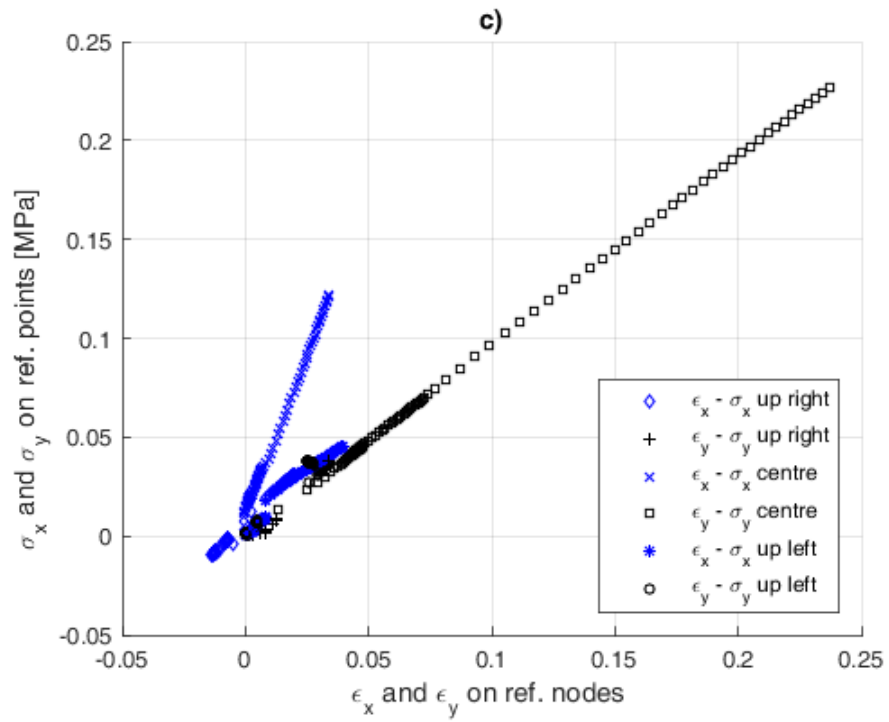(e) Intermediate Stage

(f) Final Stage

Figure 7 – a) Radial section simulated with the numerical model; b) initial stage, one-dimensional shrinkage analysis with no crack; c) intermediate stage, three-dimensional shrinkage analysis with boundary crack detected, initiated and propagated; d) final stage, three-dimensional analysis, boundary crack fully developed
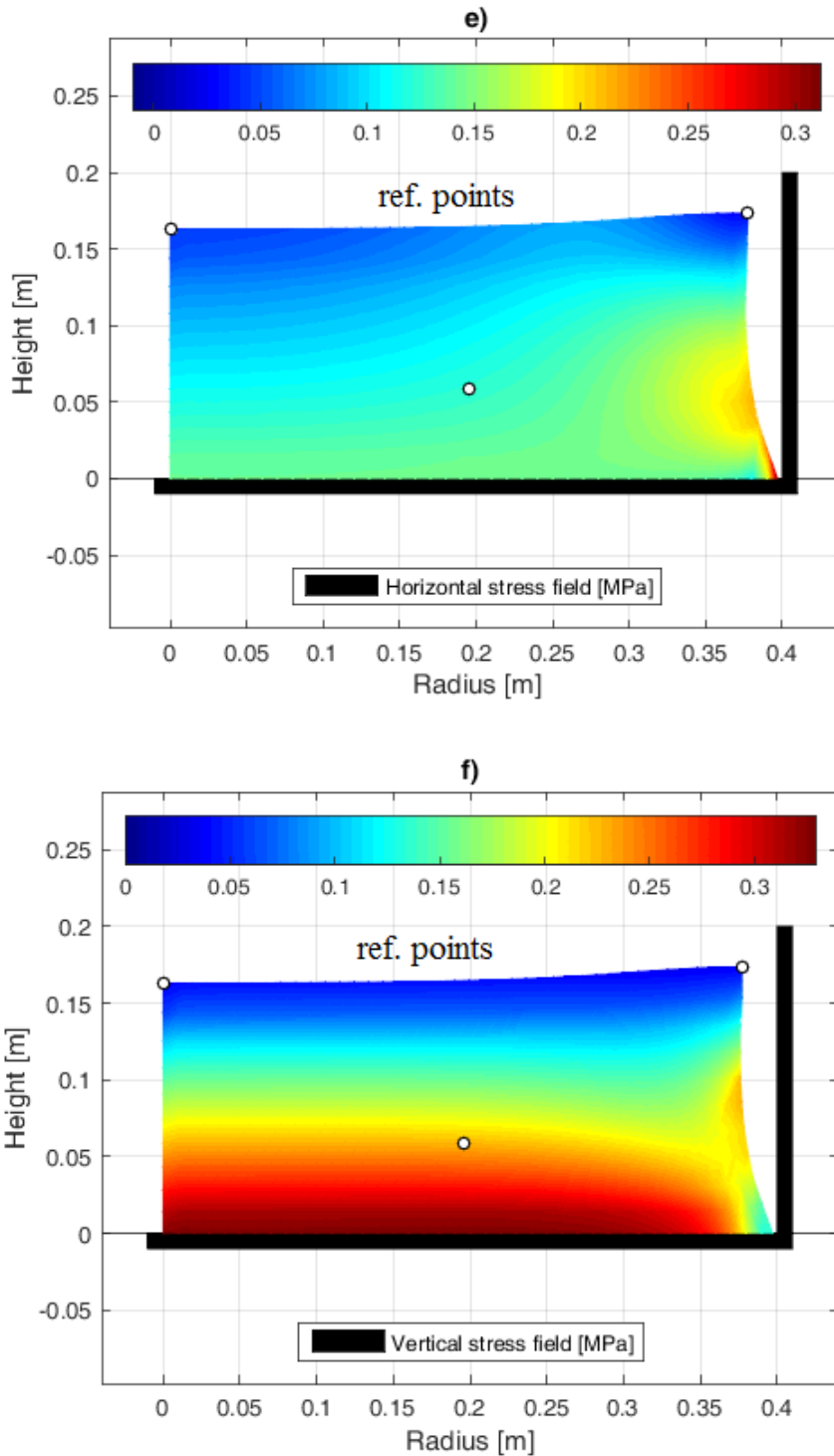
a)

b)

c)

d)

Figure 8 – Analysis using the release-node technique, starting with the Initial Stage Scheme with variable pore water pressure boundary condition: a) evolution of negative pore water pressure with time at the reference point shown in (d); b) evolution of horizontal (blue) and vertical (black) stresses with time at three reference points shown in (e) and (f); c) horizontal (blue) and vertical (black) stress-strain relation evolution at three reference points: upper-right, centre, lower-left; d) pore water pressure field, at 100 days of desiccation, on deformed radial section; e) horizontal stress field, at 100 days of desiccation, on deformed section; f) vertical stress field, at 100 days of desiccation, on deformed section

References

[1] Rodríguez RL. Estudio experimental de flujo y transporte de cromo, níquel y manganeso en residuos de la zona minera de Moa (Cuba): influencia del comportamiento hidromecánico [Ph.D. thesis]: UPC-BarcelonaTech, 2002.

[2] Rodríguez RL, Sánchez MJ, Ledesma A, Lloret A. Experimental and numerical analysis of a mining waste desiccation. Canadian Geotechnical Journal. 2007;44:644-658.

[3] Tang C-S, Shi B, Liu C, Zhao L, Wang B. Influencing factors of geometrical structure of surface shrinkage cracks in clayey soils. Engrg Geology. 2008;101(3-4):204-217.

[4] Justo JL, Vázquez NJ, Justo E. Subsidence in saturated-unsaturated soils: application to Murcia (Spain). In: Jucá JFT, de Campos TMP, Marinho FAM, editors. Third International Conference on Unsaturated Soils. Recife, Brasil, Balkema, 2002. p. 845-850.

[5] Bronswijk JJB. Modeling of water balance, cracking and subsidence in clay soils. Journal of Hydrology. 1988;97(3-4):199-212.

[6] Corte A, Higashi A. Experimental research on desiccation cracks in soil. Wilmette, Illinois, USA, 1960.

[7] Levatti HU. Estudio experimental y análisis numérico de la desecación en suelos arcillosos [Ph.D. Thesis]: UPC-BarcelonaTech, 2015.

[8] Lakshmikantha MR, Prat PC, Ledesma A. Experimental evidences of size-effect in soil cracking. Canadian Geotechnical Journal. 2012;49(3):264-284.

[9] Varsei M, Miller GA, Hassanikhah A. Novel approach to measuring tensile strength of compacted clayey soil during desiccation. Int J Geomechanics. 2016;16(6):D4016011.

[10] Lakshmikantha MR, Prat PC, Tapia J, Ledesma A. Effect of moisture content on tensile strength and fracture toughness of a silty soil. In: Toll DG, Augarde CE, Gallipoli D, Wheeler SJ, editors. Unsaturated Soils: Advances in Geo-Engineering, CRC Press/Balkema, Leiden, The Netherlands, 2008. p. 405-409.

[11] Hueckel T. On effective stress concept and deformation in clays subjected to environmental loads: Discussion. Canadian Geotechnical Journal. 1992;29:1120-1125.

[12] Lakshmikantha MR. Experimental and theoretical analysis of cracking in drying soils [Ph.D. Thesis]: UPC-BarcelonaTech, 2009.

[13] Kindle EM. Some factors affecting the development of mud-cracks. Journal of Geology. 1917;25:135-144.

[14] Haines W. The volume-changes associated with variations of water content in soil. Journal of Agricultural Science. 1923;13:296-310.

[15] Jahn A. Peculiar polygonal markings on the meadows in the Wieprz river valley. Acta Geologica Polonica. 1950;1(2):150-157.

[16] Knechtel MM. Pimpled plains of Eastern Oklahoma. Bulletin of the Geological Society of America. 1952;63:689-700.

[17] Lachenbruch AH. Depth and spacing of tension cracks. Journal of Geophysical Research. 1961;66(12):4273-4292.

[18] Lambe T. The structure of compacted clay. J Soil Mech and Found Div. 1958;84(2):1-34.

[19] Longwell CR. Three common types of desert mud cracks. American Journal of Science. 1928;15:136-145.

[20] Simpson WE. Foundation experience with clay in Texas. Civil Engineering. 1936;4:581-584.

[21] Skempton AW, Northey RD. The sensitivity of clays. Géotechnique. 1952;3(1):100-106.

[22] White WA. Colloid phenomena in sedimentation of argillacious rocks. Journal of Sedimentary Petrology. 1961;31:560-570.

[23] Willden R, Mabey DR. Giant desiccation fissures on the Black Rock and Smoke Creek deserts, Nevada. Science. 1961;133:1359-1360.

[24] Kodikara J, Barbour SL, Fredlund DG. Desiccation cracking of soil layers. In: Rahardjo H, Toll DG, Leong EC, editors. Unsaturated Soils for Asia, Balkema, 2000. p. 693-698.

[25] Ávila G. Estudio de la retracción y el agrietamiento de arcillas. Aplicación a la arcilla de Bogotá [Ph.D. Thesis]: UPC-BarcelonaTech, 2004.

[26] Chertkov VY. Modelling cracking stages of saturated soils as they dry and shrink. European Journal of Soil Science. 2002;53:105-118.

[27] Hu LB, Hueckel T, Péron H, Laloui L. Modeling Evaporation, Shrinkage and Cracking of Desiccating Soils. In: Singh B, editor. IACMAG 12. Goa, India, IIT Mumbai, 2008. p. 1083-1090.

[28] Kodikara JK, Nahlawi H, Bouazza A. Modelling of curling in desiccation clay. Canadian Geotechnical Journal. 2004;41:560-566.

[29] Lakshmikantha MR, Prat PC, Ledesma A. Characterization of crack networks in desiccating soils using image analysis techniques. In: Pande GN, Pietruszczak S, editors. Numerical Models in Geomechanics X, Balkema, 2007. p. 167-176.

[30] Lakshmikantha MR, Prat PC, Ledesma A. Image analysis for the quantification of a developing crack network on a drying soil. Geotech Test J. 2009;32(6):505-515.

[31] Lakshmikantha MR, Prat PC, Ledesma A. Evidences of hierarchy in cracking of drying soils. ASCE Geotechnical Special Publication. 2013;231:782-789.

[32] Lau JTK. Desiccation cracking of clay soils [M.S. Thesis]: University of Saskatchewan, Canada, 1987.

[33] Morris PH, Graham J, Williams DJ. Cracking in drying soils. Canadian Geotechnical Journal. 1992;29:263-277.

[34] Nahlawi H, Kodikara J. Laboratory experiments on desiccation cracking of thin soil layers. Geotechnical and Geological Engineering. 2006;24(6):1641-1664.

[35] Péron H, Hueckel T, Laloui L, Hu LB. Fundamentals of desiccation cracking of fine-grained soils: experimental characterisation and mechanisms identification. Canadian Geotechnical Journal. 2009;46(10):1177-1201.

[36] Tang C-S, Shi B, Liu C, Gao L, Inyang H. Experimental Investigation of the Desiccation Cracking Behavior of Soil Layers during Drying. J Mat Civil Engrg. 2011;23(6):873-878.

[37] Tang C-S, Shi B, Liu C, Suo W-B, Gao L. Experimental characterization of shrinkage and desiccation cracking in thin clay layer. Applied Clay Science. 2011;52(1-2):69-77.

[38] Vogel HJ, Hoffmann H, Roth K. Studies of crack dynamics in clay soil. I: Experimental methods, results and morphological quantification. Geoderma. 2005;125(3-4):203-211.

[39] Trabelsi H, Jamei M, Zenzri H, Olivella S. Crack patterns in clayey soils: Experiments and modeling. Int J Num Anal Methods in Geomechanics. 2012;36:1410-1433.

[40] Sima J, Jiang M, Zhou C. Modeling desiccation cracking in thin clay layer using three-dimensional discrete element method. Proceedings American Institute of Physics. 2013;1542(1):245-248.

[41] Amarasiri AL, Kodikara J, Costa S. Numerical modelling of desiccation cracking. Int J Num Anal Methods in Geomechanics. 2011;35:82-96.

[42] Sánchez M, Manzoli OL, Guimarães LN. Modeling 3-D desiccation soil crack networks using a mesh fragmentation technique. Computers and Geotechnics. 2014;62:27-39.

[43] Gui Y, Zhao GF. Modelling of laboratory soil desiccation cracking using DLSM with a two-phase bond model. Computers and Geotechnics. 2015;69:578-587.

[44] Zienkiewicz OC, Chan AHC, Pastor M, Paul DK, Shiomi T. Static and Dynamic Behaviour of Soils: A Rational Approach to Quantitative Solutions. I. Fully Saturated Problems. Proceedings of the Royal Society of London Series A, Mathematical and Physical Sciences. 1990;429(1877):285-309.

[45] Matyas EL, Radhakrishna HS. Volume change characteristics of partially saturated soils. Géotechnique. 1968;18(4):432-448.

[46] Lloret A, Alonso EE. State surfaces for partially saturated soils. XI International Conference on Soil Mechanics and Foundation Engineering. San Francisco, Balkema, 1985. p. 557-562.

[47] Barrera M. Estudio experimental del comportamiento hidro-mecánico de suelos colapsables [Ph.D. Thesis]: UPC-BarcelonaTech, 2002.

[48] Anandarajah A. Computational Methods in Elasticity and Plasticity. Solid and Porous Media. Springer 2010.

[49] Lee FH, Lo KW, Lee SL. Tension crack development in soils. Journal of Geotechnical Engineering ASCE. 1988;114(8):915-929.

[50] Konrad J-M, Ayad R. An idealized framework for the analysis of cohesive soils undergoing desiccation. Canadian Geotechnical Journal. 1997;34:477-488.

[51] Lakshmikantha MR, Prat PC, Ledesma A. An experimental study of cracking mechanisms in drying soils. In: Thomas HR, editor. Environmental Geotechnics V. London: Thomas Telford, 2006. p. 533-540.

[52] Lakshmikantha MR, Prat PC, Ledesma A. Boundary effects in the desiccation of soil layers with controlled environmental conditions. Geotechnical Testing Journal. 2018; 41 (4).

[53] Levatti HU, Prat PC, Ledesma A, Cuadrado A, Cordero J. Experimental analysis of 3D cracking in drying soils using Ground Penetrating Radar. Geotech Test J. 2017;40(2):221-243.

[54] Prat PC, Ledesma A, Cuadrado A, Levatti HU. Ground penetrating radar system for detection of desiccating cracks in soils. In: Pietruszczak S, Pande GN, editors. ComGeo-III. Kraków, Poland, International Centre for Computational Engineering, 2013. p. 249-258.

[55] van Genuchten MT. Closed-form equation for predicting the hydraulic conductivity of unsaturated soils. Soil Science Society of America Journal. 1980;44(5):892-898.

[56] Burland JB. Some aspects of the mechanical behaviour of partly saturated soil. Moisture Equilibrium and Moisture Changes in Soils Beneath Covered Areas. Sydney, Butterworths, 1965. p. 270-278.

[57] Bishop AW, Blight GE. Some aspects of effective stress in saturated and partly saturated soils. Géotechnique. 1963;13(3):177-197.

[58] Blight GE. A study of effective stresses for volume change. Moisture Equilibrium and Moisture Changes in Soils Beneath Covered Areas. Sydney, Butterworths, 1965. p. 259-269.

[59] Aitchison GD. Soil properties, shear strength, and consolidation. 6th Conference SMFE1965. p. 319-321.

[60] Jennings J, Burland JB. Limitations to the use of effective stress in partly saturated soils. Géotechnique. 1962;12(2):125-144.

[61] Richards LA. Capillary conduction of liquids through porous mediums. Physics. 1931;1:318-333.

[62] Kuna M. Finite Element in Fracture Mechanics. Theory, numerics and applications. Springer 2013.

[63] Griffith AA. The phenomenon of rupture and flow in solids. Phil Trans Roy Soc London. 1921;Ser. A(221):163-198.

[64] Griffith AA. The theory of rupture. 1st Int Congr Appl Mech. Delft1924. p. 55-63.

[65] Lewis RW, Schrefler BA. The Finite Element Method in the Static and Dynamic Deformation and Consolidation of Porous Media. 2 ed: Wiley, 1998.

Appendix

The *u-p* formulation

In the *u-p* formulation [44], where $\mathbf{u}$ are the nodal displacements and $\mathbf{p}$ is the nodal negative porewater pressure, the problem of desiccation, which is a hydro-mechanical problem, is expressed in matrix form by the set of partial differential equations:

$$
\begin{bmatrix} \mathbf{0} & \mathbf{0} \\ \mathbf{0} & \mathbf{H} \end{bmatrix} \begin{bmatrix} \overline{\mathbf{u}} \\ \overline{\mathbf{p}} \end{bmatrix} + \begin{bmatrix} \mathbf{K}_T & \mathbf{Q}_T \\ \mathbf{P} & \mathbf{S} \end{bmatrix} \begin{bmatrix} \dfrac{d\overline{\mathbf{u}}}{dt} \\ \dfrac{d\overline{\mathbf{p}}}{dt} \end{bmatrix} = \begin{bmatrix} \dfrac{d\mathbf{f}^u}{dt} \\ \mathbf{f}^p \end{bmatrix}
$$

where the tangent matrices of the stress-strain problem are:

Stiffness Matrix:
$$ \mathbf{K}_T = \int_\Omega \mathbf{B}^\mathrm{T} \mathbf{D} \mathbf{B} \, d\Omega $$

Coupling Matrix:
$$ \mathbf{Q}_T = \int_\Omega \frac{1}{3\mathbb{K}_t^s} \mathbf{B}^\mathrm{T} \mathbf{D} \mathbf{m} \mathbf{N}_\mathrm{p} \, d\Omega $$

Vector of Nodal Forces:
$$ \frac{\partial \mathbf{f}^u}{\partial t} = \int_\Omega \mathbf{N}_u \rho \frac{\partial \mathbf{g}}{\partial t} \, d\Omega + \int_\Omega \mathbf{N}_u \frac{\partial \overline{\mathbf{t}}}{\partial t} \, d\Omega $$

And the matrices of the flow problem are:

Coupling Matrix:
$$ \mathbf{P} = \int_\Omega \left(\mathbf{N}_\mathrm{p}\right)^\mathrm{T} S_r \, \mathbf{m}^\mathrm{T} \mathbf{B} d\Omega $$

Compressibility Matrix:
$$ \mathbf{S} = \int_\Omega \left(\mathbf{N}_\mathrm{p}\right)^\mathrm{T} n \frac{\partial S_r}{\partial u_w} \mathbf{N}_\mathrm{p} \, d\Omega + \int_\Omega \left(\mathbf{N}_\mathrm{p}\right)^\mathrm{T} \frac{n S_r}{K^w} \mathbf{N}_\mathrm{p} \, d\Omega $$

Permeability Matrix:
$$ \mathbf{H} = \int_\Omega \left(\nabla \mathbf{N}_\mathrm{p}\right)^\mathrm{T} \mathbf{K}(S_r) \nabla \mathbf{N}_\mathrm{p} \, d\Omega $$

Vector of Nodal Flow:
$$ \mathbf{f}^p = \int_\Omega \rho^w \left(\nabla \mathbf{N}_\mathrm{p}\right)^\mathrm{T} \mathbf{K}(S_r) \mathbf{g} \, d\Omega - \int_\Gamma \left(\mathbf{N}_\mathrm{p}\right)^\mathrm{T} q^w \, d\Gamma $$

Where $\mathbf{N}_p$, and $\mathbf{N}_u$ are shape functions for the suction and displacements on the finite element mesh nodes. $\mathbf{B}$ is a transformation matrix derived from the finite element method [44].

Variables and parameters of the numerical model

$\boldsymbol{\sigma}$: total stress tensor

$\boldsymbol{\sigma}^{net}$: net stress (stress in excess of air pressure)

s : suction

t : time

u_a: air pore pressure

u_w : water pore pressure

$\boldsymbol{\varepsilon}$: total strain

ε_v^{net}: net volumetric strain

ε_v^s : suction volumetric strain

$\boldsymbol{\varepsilon}^s$: spherical tensor of deformations due to suction ($\varepsilon_{ij}^s = u_w \delta_{ij}/K_t^s$)

$\mathbf{u}$: displacements

$\mathbf{D}$: 4th order tangent stiffness tensor

$\mathbf{C}$: 4th order compliance tensor

$\mathbf{h}$: 2nd order tensor related to changes in suction

$\mathbb{K}$: volumetric modulus of the soil matrix

$\mathbb{G}$: shear modulus of the soil matrix

$\mathbb{K}^s$: volumetric suction modulus

$\mathbf{1} \equiv \delta_{ij}$: identity tensor.

Δe : void ratio increment

n : soil porosity

$\{a_1, a_2, a_3, a_4\}$: state surface parameters calibrated from laboratory tests

σ_m^{net}: mean net stress

p_{ref} : reference pressure to avoid logarithm indeterminacy

$\mathbf{q}$: Darcy's velocity vector

∇u_w: porewater pressure gradient

$\mathbf{K}$: permeability tensor

S_r: water saturation degree

$\mathbf{g}$: gravity vector

ρ^w: water density

k^{rl} : non-dimensional relative permeability

r , b and λ : material parameters

μ^l: temperature-dependent dynamic viscosity of water

$\mathbf{k}$: intrinsic permeability tensor

γ_w: specific weight of water

K: hydraulic conductivity of the soil

K^w: water compressibility

k_0: saturated hydraulic conductivity of reference at $n = n_0$

k_{sat}: saturated hydraulic conductivity for porosity n

P_0: air entry value for the initial porosity n_0

f_n: function that takes into account the influence of porosity in the retention curve by means of parameter η

ρ : soil unit weight

ρ^w : water unit weight

$\boldsymbol{w_S}$: shrinkage limit

$\boldsymbol{w_L}$: liquid limit

$\boldsymbol{w_P}$: plastic limit

$\boldsymbol{PI}$: plasticity index

Finite Element Method Matrices and Vectors

$\mathbf{u}$: nodal displacements

$\mathbf{p}$: nodal negative porewater pressure

$\mathbf{K}_T$: global stiffness matrix

$\mathbf{Q}_T$ and $\mathbf{P}$: coupling matrices

$\mathbf{S}$: compressibility matrix

$\mathbf{H}$: permeability matrix

$\mathbf{N}_p$ and $\mathbf{N}_u$: pressure and displacement shape functions

$\mathbf{B}$: transformation matrix derived from the finite element method

$\mathbf{m} = [1 \quad 1 \quad 1 \quad 0 \quad 0 \quad 0]^T$: identity tensor in vector form

Ω : domain

Γ : contour